Chapter 15
Nanostructured Surfaces of Doped Alkali Halides

Clemens Barth

Abstract In this Chapter, we explore the fascinating world of the nanostructured (001) Suzuki surface of Mg^{2+} and Cd^{2+} doped NaCl single crystals—surfaces that have been recently rediscovered by noncontact AFM and Kelvin probe force microscopy in ultra-high vacuum. The surface morphology, the atomic surface structure and the identification of surface ions will be discussed. At the end of this Chapter two applications exemplify a nanostructured growth of functionalized molecules with polar substituents and metal nanoparticles on the Suzuki surface.

15.1 Introduction

Alkali halides have been extensively studied in condensed matter physics [1], and the crystal and electronic structure, optical properties, defects, doping, the ionic conductivity and surface reactivity related phenomena have been addressed already several decades ago [2, 3]. Before atomic force microscopy (AFM) was introduced in 1986 [4], the morphology of the (001) surface has been mainly studied by the combination of the gold decoration method and transmission electron microscopy (TEM), starting from the end of the 1950s [5, 6]. Such studies gave great insights into diffusion and evaporation related surface phenomena [7–9] as well as into impurity controlled surface modifications [10–12] . After the introduction of frequency modulated noncontact AFM (nc-AFM) [13–16], the surfaces of alkali halides have become yet again *standard model surfaces*. The atomic structure [17–25], defect identification [26–28], indentation [29] as well as adsorbed molecules [30, 31], self-assembled molecules [32–41] but also metal NPs [40, 42–48] have been addressed. In recent revolutionary work, alkali halide thin films have been used to support single molecules for imaging their atomic structure with an unmatched resolution [49–54].

The reason for the extensive use of alkali halide surfaces in nc-AFM is that they can be easily prepared in ultra-high vacuum (UHV): for instance, cleaving a single

C. Barth (✉)
Aix-Marseille Université, CNRS, CINaM UMR 7325,
Campus de Luminy, Case 913, 13288 Marseille Cedex 09, France
e-mail: barth@cinam.univ-mrs.fr

S. Morita et al. (eds.), *Noncontact Atomic Force Microscopy*,
NanoScience and Technology, DOI 10.1007/978-3-319-15588-3_15

crystal along the (001) cleavage plane, which is mostly followed by in-situ annealing at moderate temperatures (∼100 °C) [26, 55, 56], is completely sufficient to obtain clean surfaces with large atomically and stoichiometric flat terraces—ideal conditions for nc-AFM and KPFM. The imaging with atomic resolution and of supported molecules or metal nanoparticles can be easily accomplished. A very important property is that alkali halide surfaces are quite inert in UHV such that measurements can be done within a week during which the surface remains almost clean. Another advantage is that the number of possible defects, which are stable during the acquisition time of AFM experiments, is quite limited: apart from impurities, F^0 centers (anion vacancy with a localized electron inside), cation and anion vacancies are the only candidates. This helps the interpretation of surface phenomena observed by nc-AFM where defects play a fundamental role. Note that high-quality alkali halide surfaces can also be obtained by evaporating a small amount of the alkali halide material onto almost any clean and atomically flat substrate surface (thin alkali halide films) like on silver [57, 58], copper [59, 60], HOPG [61] and even silicon surfaces [62].

Apart from all the latter advantages there is another one of general importance: alkali halides can be easily doped with divalent metal impurity ions such as Mg^{2+} or Cd^{2+}, via adding the respective salt into the melt during the growth of an alkali halide crystal (e.g., $CdCl_2$ or $MgCl_2$ in NaCl, see [63]). Such impurities replace the standard cations and create a cation vacancy in their vicinity to guarantee charge neutrality within the crystal. At specific doping concentrations, new phases with new atomic structures inside the alkali halide can be created. One of such phases is the Suzuki phase discovered by Kazuo Suzuki in 1961.

In this Chapter, we will see that NaCl crystals, which are doped with 1–5 % MgCl or $CdCl_2$, exhibit nanostructured surfaces with two distinct surface regions: one from pure NaCl and one from the Suzuki structure. The surface morphology, which was studied as a function of surface preparation (annealing, impurity concentration, etc.), atomic resolution imaging including identification of surface ions and applications of the surface in the domain of molecular self-assembly and heterogeneous model catalysis will be discussed.

To complete the picture of *doped alkali halides in nc-AFM*, we first describe the surfaces of those alkali halide crystals, which are often referred as to *crystals of highest purity*, and crystals that contain only a few impurity ions (< 1 %). We will see that impurities at low doping level sensitively determine the charge state of the surface by creating a Debye-Frenkel dipole layer at the surface.

15.2 Low Defect Concentration—the Debye-Frenkel Layer

For many nc-AFM experiments, alkali halide crystals of highest purity are purchased from crystal growing companies. When such single crystals are cleaved in UHV, some surface charge is generally detected even at large distances of several tens and hundreds of nanometer, depending on the cleavage [56]. In literature it is quite often mentioned that prior to AFM experiments a crystal is annealed at temperatures

around 100 °C to 'remove the surface charge', which was produced by the cleavage. A fundamental question has been always if all surface charge is removed after the annealing and if the surface is defect-free. To give answers to this question, KPFM can be used because it is sensitive on surface charges and their lateral distribution [26, 64, 65].

Surprisingly, after a preparation by UHV cleavage and annealing KPFM images always show a contrast, which is stable and does not change by time. Apart from a very faint, over large distances smoothly varying Kelvin contrast [56] a very localized, sharp contrast at the steps is regularly observed [26–28] (Fig. 15.1a, b). The latter type of contrast is composed of single round patches, which have a lateral dimension typically of 10–20 nm [26]. Because of the high purity no material other than alkali halide is present on the surface so that the contrast is due to localized charged defects, which change the local electrostatic surface potential at the steps. It is clear that such defects cannot 'aggregate' into nanometer large structures. And indeed, atomic resolution imaging regularly reveals atomic sized defects at the kink and corner sites of steps, exactly at the position of the patches in the Kelvin image [26]. For instance, the defects 1 and 2 at the two kinks in Fig. 15.1c are exactly located at the bright patch (yellow circle) in image Fig. 15.1a, b. Such 'charged defects' are a point source in the KPFM contrast formation: because of its long-range character the electrostatic force is detected by the whole tip apex such that the shape of the apex is imaged

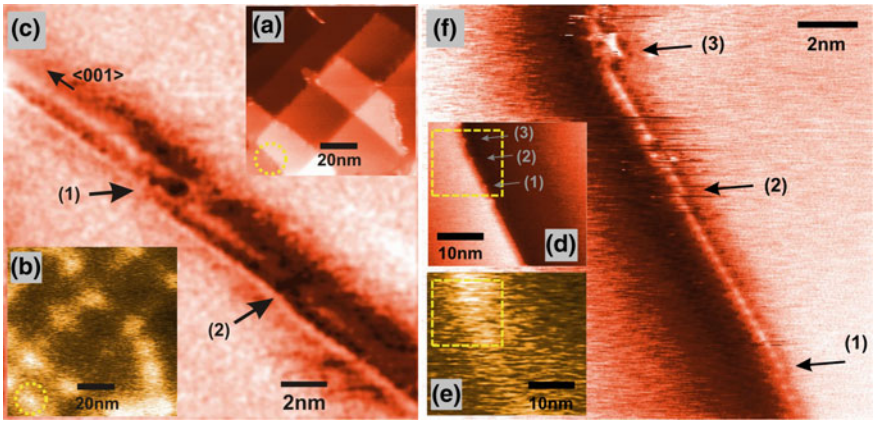

Fig. 15.1 The Debye-Frenkel-Layer on alkali halide crystal surfaces. **a–c** Topography (**a**) and Kelvin image (**b**) simultaneously recorded on the (001) surface of a KCl crystal of highest purity (Kelvin contrast: $U_{step-terrace} = +0.4$ V). **c** Constant height image recorded in the surface region marked by the *dotted circle* in **a**. **d–f** Topography (**d**) and Kelvin image (**e**) simultaneously recorded on a (001) surface of a NaCl crystal, which was doped with 0.1 % $MgCl_2$ (Kelvin contrast: $U_{step-terrace} = +0.3$ V). **f** Constant height image recorded in the surface region marked by the *dotted square* in **d**. The bright patches in the Kelvin images (**b**) and (**e**) correspond to more negative surface sites with respect to the neutral alkali halide terraces. The negative surface sites are created by cation vacancies at kink and corner sites of steps as verified by atomic resolution (**c**) and (**f**) at the respective places. Both crystals were cleaved in UHV and annealed at 150–200 °C (From [26])

when the tip scans a charged defect. This explains the size of the patches but also the observation that in a Kelvin image all patches have the same size.

The most important observation is that the patches always exhibit the same contrast at the steps (e.g., always a bright contrast), which corresponds to a net negative surface charge [26–28]. In fact, it documents a fundamental property of the surfaces of ionic material in condensed matter physics, and is refereed to as the *Double layer* or *Debye-Frenkel layer* introduced by Frenkel in 1946 [66, 67]: if for an ideal pure crystal (no impurities) the free formation energies for the creation of anion and cation vacancies are different in the near surface region, an excess of one type of vacancy is generated by time. Because, e.g., a cation vacancy has 6 or 5 neighboring anions in the bulk or on the terrace, respectively, (anion vacancy: 6 or 5 neighboring cations) it is a very negative site carrying a 'negative charge' (anion vacancy: 'positive charge'). Therefore, an excess of one type of vacancy would charge up the crystal, which is an impossible scenario. A mechanism is therefore needed that balances this excess charge. In fact, a double layer is created such that one type of vacancy is located on the surface whereas the other one is stabilized in a layer below the surface, in a so-called *space charge layer* [68–71]. Both layers form a dipole that modifies the free formation energy for the creation of cation and anion vacancies, which finally balances the electrostatics of the crystal [72]. Note that the free formation energies for anion and cation vacancy creation are indeed different on the surface and strongly depend on the temperature [72]: when monotonously changing the temperature (e.g., from low to high temperatures) the surface charge may become zero and switch its sign, which means that the vacancies change the respective layer. This was verified by a couple of experiments for different alkali halide crystals, explicitly showing a surface charging in dependence on temperature [72].

With respect to the surface site of the vacancies, calculations have shown that the vacancies find their energetic equilibrium position at especially low-coordinated surface sites, which are the kink and corner sites of steps [43, 73, 74]. Because alkali halide crystals are generally annealed prior to nc-AFM experiments the probability to find vacancies at steps is therefore high due to the high mobility of vacancies at room and in particular at elevated temperatures [43, 75].

The latter description of the Debye-Frenkel layer is in fact the *intrinsic case* [68], which is valid for high temperatures only when considering crystals of even highest purity. However, at relatively low temperatures like at room temperature, the so-called *extrinsic case* predominates due to the presence of impurities, which have valences other than +1 or −1 [69]. In fact, any real alkali halide crystal of even highest available purity does contain impurities. In most cases, the crystals contain divalent metal impurity ions like Ca^{2+} or Mg^{2+}. Because of the different valence with respect to the host cations, negative cation vacancies are created in order to conserve charge neutrality. At thermal equilibrium, a Debye-Frenkel layer is created such that the net negative surface charge of the cation vacancies on the surface is compensated by the positive impurities below the surface. Note that already a very small impurity amount of only a few ppm is sufficiently large to create a Debye-Frenkel layer. Furthermore, note that it is difficult to introduce divalent negative impurities, which would lead to

positive anion vacancies. Therefore, a net negative surface charge is created at room temperature by negative cation vacancies only [69].

The ultimate experiment to investigate the Debye-Frenkel layer is to examine the charge state of alkali halide crystals, which are *explicitly* doped with divalent metal impurity ions. In the case of such doped alkali halides, same type of observations must be made and even more, the density of the negative sites at the steps should increase upon an increase of the impurity content, as indeed observed on the (001) surfaces of Mg^{2+} and Cd^{2+} doped NaCl crystal surfaces (Fig. 15.1d–f).

The Debye-Frenkel layer is a fundamental property for surfaces of any ionic material. For instance, a Debye-Frenkel layer could also be observed on the (111) surface of CaF_2 by nc-AFM and KPFM [76]. Not only can the surface acts as a source or sink for charged defects but also dislocations and grain boundaries [67, 77]. In the case of dislocations, the dislocation line carries one type of charge and is surrounded by a symmetric space charge cloud of opposite charge. Charged dislocations could be indeed observed by nc-AFM and KPFM experiments on the (001) surface of bulk KBr, where dislocations were explicitly created by nanoindentation experiments [27].

15.3 High Defect Concentration—The Suzuki Phase

When the amount of divalent impurity cations in alkali halides is increased in the ppm range the (001) surface increases the number of negative vacancies at steps, building up a stronger Debye-Frenkel layer. However, at an impurity content of roughly 1 % a new important mechanism in condensed matter physics takes place inside the crystal:precipitation of impurities into new structures, which are localized in small regions inside the otherwise unchanged pure alkali halide. One important phase amongst others (see [63, 78] for a brief overview) is the so-called *Suzuki phase*, which appears in alkali halides in a doping range between roughly 1 and 10 %. The Suzuki phase was first found in Cd^{2+} doped NaCl (NaCl:Cd^{2+}) by the Japanese Kazuo Suzuki in 1961 thanks to his X-ray diffraction experiments [78]. Apart from the Suzuki phase in NaCl:Cd^{2+} crystals [12, 63, 78–92] the same phase was discussed for Mn^{2+} [10, 11, 63, 82, 83, 86, 88, 90, 93–100], Mg^{2+} [22, 63, 82, 89, 90], Fe^{2+} [11, 63, 82, 86, 90, 101, 102], Ni^{2+} [63, 103], Co^{2+} [104], Sr^{2+} [63, 105] and Pb^{2+} [63, 106] doped NaCl crystals. The host lattice must not necessarily be NaCl, the Suzuki phase may exist also in NaBr (Mn^{2+} [100]), KCl (Sm^{2+} [107], Pb^{2+} [108], Eu^{2+} [109, 110]), KBr (Mn^{2+} [111], Eu^{2+} [110, 112, 113]), LiF (Mg^{2+} [114, 115]), AgCl (Pb^{2+} [116]) and even in oxides (MgO:Mn^{2+} [117–120], NiO:Mn^{2+} [120], CuO:Pb^{2+} [121, 122]). Suzuki phases including two types of metal impurity cations were also found (NaCl:Pb, Eu^{2+} [123] and NaCl:Cd, Pb^{2+} [124]).

In the following, we discuss the Suzuki structure for NaCl crystals. The morphology of the respective (001) surface and atomic resolution imaging in conjunction with the identification of surface ions and vacancies are involved. The Section shall demonstrate that by using nc-AFM and KPFM very important surface properties of doped alkali halide crystals can be characterized.

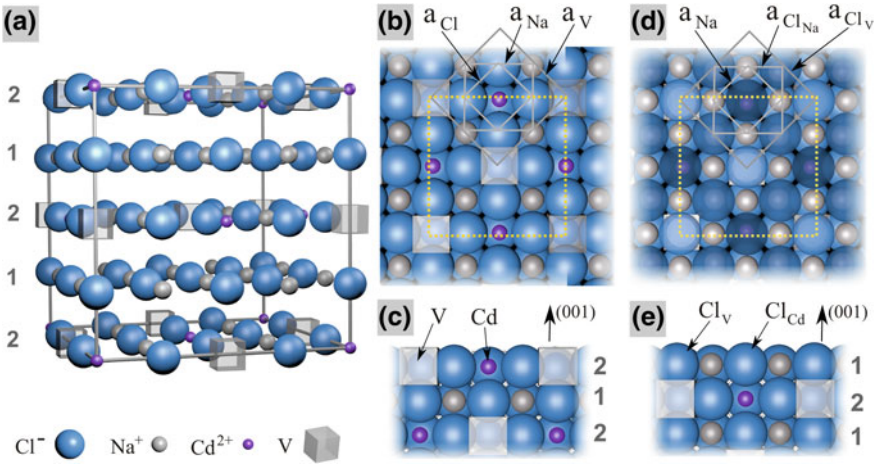

Fig. 15.2 The atomic structure of the Suzuki phase, exemplified for Cd^{2+} doped NaCl. **a** The Suzuki unit cell is almost two times larger ($a_S = 11.24$ Å) than the one of NaCl ($a_{NaCl} = 5.64$ Å) [78]. **b** *Top view* with a projection of the Suzuki unit cell (*yellow dotted square*) on the Suzuki terminated (001) surface. The Cd^{2+} ions and the vacancies form each a sub-lattice with a size of $a_V = a_{Cd^{2+}} = a_S/\sqrt{2}$, which is larger than the sub-lattices of the Na^+ ($a_{Na^+} = a_S/2$) and Cl^- ions ($a_{Cl^-} = a_S/2\sqrt{2}$). **c** *Side view* of the Suzuki terminated (001) surface. **d** *Top view* on the NaCl terminated (001) surface with chlorines above the vacancies (*bright blue*, Cl_V^-), Na^+ ions (*blue*, Cl_{Na}^-) and Cd^{2+} ions (*dark blue*, Cl_{Cd}^-). The Cl_V^- and Cl_{Cd}^- ions form each a sub-lattice with dimension $a_V = a_{Cl_V} = a_{Cl_{Cd}} = a_S/\sqrt{2}$ whereas the Cl_{Na}^- form a smaller sub-lattice with the size $a_{Cl_{Na}} = a_S/2$. The Na^+ ions form the smallest sublattice ($a_{Na^+} = a_S/2\sqrt{2}$). **e** *Side view* of the NaCl terminated (001) surface

15.3.1 Structure and Surface of the Suzuki Phase

The unit cell of the Suzuki phase is cubic and almost twice as large as the one of the corresponding alkali halide (Fig. 15.2a) [78, 91]. The structure is composed of alternating layers of pure NaCl (layer 1) and layers, which include the regular Cl^- ions, a part of the regular Na^+ ions, the positive divalent Cd^{2+} impurities and Na^+ vacancies for compensating the additional positive valence of the impurities (layer 2). Due to the specific structure, the composition is given either by $CdCl_2{\cdot}6NaCl$ or simply Na_6CdCl_8 for Cd in NaCl. Although the size of the unit cell of the Suzuki phase can be precisely measured by X-ray diffraction, slightly deviating values for its size were reported. For NaCl:Cd^{2+} crystals a size between 11.248(3) Å [82] and 11.278 Å [85] was found, which is slightly smaller than the value of 11.39(1) Å calculated at 0 Kelvin [91, 92]. The experimental values show that the Suzuki unit cell is slightly smaller than the double size of the NaCl unit cell, with a mismatch around 0.15 % ($a_{NaCl} = 5.64$ Å, $a_{Suzuki}/2 = 5.624$ Å [82], $a_{Suzuki}/2 = 5.639$ Å [85]). However, thanks to this very small lattice mismatch the Suzuki structure exists in up to 1 μm^3 large cubic precipitates inside real crystals, almost perfectly incorporated in the pure NaCl matrix [89].

With respect to the (001) surface, two possible surface terminations exist: either the surface is terminated by a layer containing regular Na^+ and Cl^- ions, the impurities and vacancies (*Suzuki-termination* , Fig. 15.2b, c) or by a pure NaCl layer (*NaCl-termination*, Fig. 15.2d, e). On the NaCl-terminated surface, the Na^+ ions are located above Cl^- ions of the second layer whereas the Cl^- ions sit either above second layer vacancies, impurities or Na^+ ions. In particular the Cl^- ions above the vacancies experience a strong outward relaxation of 40 pm while those over Cd^{2+} ions remain close to the ideal surface plane [25]. Such surface relaxations lead to a break of the NaCl surface symmetry such that several sub-latices are formed, as now explained for the Suzuki-termination (Fig. 15.2): on the Suzuki-terminated surface the Na^+, Cl^- and Cd^{2+} ions but also the vacancies form each highly symmetric sub-lattices, each of which has a precise dimension and orientation in the (001) plane. Already Kazuo Suzuki concluded from his X-ray diffraction experiments that the Cl^- ions relax towards the Cd^{2+} ions in the (001) surface plane [78], whereas the Na^+ and Cd^{2+} ions stay on the regular sites of the NaCl structure. In literature different values for the surface relaxation δ (fraction of a_{Suzuki}) of the Cl^- ions can be found (δ: 0.028 [78], 0.014 [79], 0.020 [125], 0.0154 [91]). The average of the latter values ($\delta = 0.19$) exemplifies that the Cl^- ions relax 20 pm towards the Cd^{2+} ions in the (001) surface plane.

In Sect. 15.3.3 we will see that thanks to the specific Suzuki structure an identification of all surface ions and the vacancies is possible by imaging the surface with atomic resolution in the nc-AFM mode.

15.3.2 Surface Morphology

15.3.2.1 Surfaces Prepared by Cleavage in UHV

If a doped alkali halide crystal with Suzuki precipitates inside the bulk—a so-called *Suzuki crystal*—is cleaved in UHV a flat (001) surface is obtained, which is called the *Suzuki surface*. Because the cleavage crack passes through the regular pure NaCl but also through some precipitates during the cleavage, two types of surface regions co-exist [126]: one from pure NaCl (*NaCl regions*) and one from a regular Suzuki structure (*Suzuki regions*). Figure 15.3 shows typical characteristics of the (001) surface after the UHV cleavage of a NaCl:Cd^{2+} crystal (4 Mol % of $CdCl_2$): in the middle of the topography image (Fig. 15.3a) two $400 \times 400\,\mathrm{nm}^2$ large square shaped Suzuki regions can be found, which are surrounded by regions of pure NaCl(001). The regions appear in form of depressions whereas their edges are oriented along equivalent ⟨100⟩ surface directions as observed before by TEM on surfaces of as-cleaved crystals [10, 86]. The square shape of the regions is in fact the projection of the almost cubic shape of the Suzuki precipitates onto the (001) surface [86, 94].

An important characteristic are cleavage steps inside the Suzuki regions [126]: the topography image (Fig. 15.3a) shows cleavage steps with a height of 5.6 Å implying that all terraces are either NaCl or Suzuki-terminated. The specific step structure is a

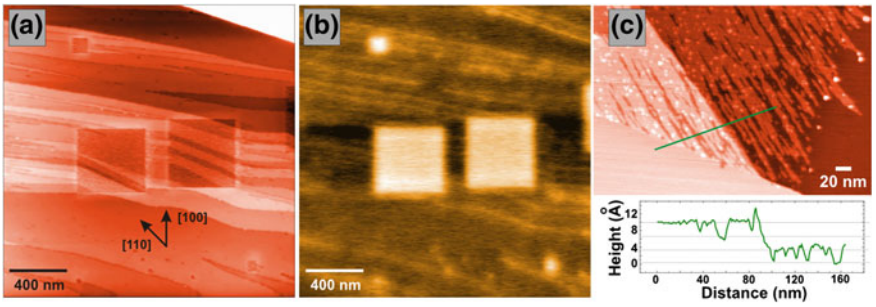

Fig. 15.3 Suzuki precipitates on the (001) surface of an as-cleaved NaCl:Cd^{2+} crystal (4 Mol % of $CdCl_2$). Topography (**a**) and Kelvin image (**b**) simultaneously recorded at a large Suzuki precipitate (Kelvin contrast of the precipitate and NaCl steps: $U_{Suzuki-NaCl_{terrace}} = +1.3$ V and $U_{NaCl_{terrace}-NaCl_{step}} \sim +0.3$ V, respectively). The $a_{Suzuki}/2 \approx 5.6$ Å high steps inside the Suzuki precipitates were created by the cleavage crack, which cut ⟨110⟩ screw dislocations at the Suzuki-NaCl. **c** Another Suzuki precipitate found on the same crystal surface. Steps with a height of only $1/4a_{Suzuki} \approx 2.8$ Å can be seen, exhibiting both, NaCl and Suzuki-terminated streaks (From [126])

result of the cleavage crack, which cuts ⟨110⟩ screw dislocations at the Suzuki-NaCl interface, which leads to ⟨100⟩ slip steps in adjacent NaCl regions. Because the unit cell of the Suzuki phase is not exactly twice that of the NaCl unit cell ($a_{NaCl} = 5.64$ Å and $a_{Suzuki}/2 = 5.624$ Å [82]), the dislocations are a result of the small misfit and release the related strain at the interface [94]. The ⟨110⟩ screw dislocations lie in the {110} planes, which intersect the (001) surface and which are the slip or gliding planes in pure NaCl [127–129]. In other Suzuki regions (Fig. 15.3c) steps with a height of only 2.8 Å $\approx 1/2a_{NaCl} \approx 1/4a_{Suzuki}$ could be found exhibiting both, NaCl and Suzuki-terminated surfaces. Such steps are probably a result of the alternating expansions and contradictions of the Cl^- ions, which appear around the Cd^{2+} ions along ⟨110⟩ directions. These alternating strains are then relieved by partial ⟨110⟩ screw dislocations, which have a magnitude of the burgers vector of $\sqrt{2}\cdot\delta\cdot a_{Suzuki}$ [86].

When KPFM is done on a Suzuki surface a strong contrast in the Suzuki regions is regularly observed, corresponding to voltage differences of one volt and more with respect to the neutral NaCl regions [22, 126] (Fig. 15.3b). The Kelvin contrast is homogeneous inside the Suzuki precipitates and no further details can be obtained even by choosing smaller scanning frames. The bright contrast is due to the high density of negative surface sites in the Suzuki regions: for instance, on the Suzuki-terminated surface a vacancy is surrounded by four Cl^- ions in the first layer and one underneath the vacancy in the second layer, which all form a negative surface site [22]. With respect to the NaCl-terminated Suzuki surface, the Cl^- ions located above the Na^+ vacancies relax by 40 pm from the surface (see Sect. 15.3.1). Such Cl^- ions can be considered as low-coordinated ions with respect to Cl^- ions above the impurities. Comparable to the negative vacancies at kinks of steps (see Sect. 15.2), both sites (vacancies and Cl^- ions above vacancies) create a more negative surface potential [26].

With respect to the uniform Kelvin contrast inside the Suzuki regions, the tip collects the electrostatic tip-surface interaction over a surface region which is comparable to the nanometer size of the tip apex, covering many negative surface sites. This explains not only the homogeneous contrast but also the high voltage difference in the volt range. On the contrary, single Na^+ vacancies at steps in pure NaCl(001) regions, which are well separated from each other, produce a considerably lower bright contrast of ∼300 mV, which is in agreement to earlier findings on pure alkali halide surfaces [26, 27] (see Sect. 15.2).

Interestingly, all Suzuki regions exhibit the same net negative surface charge in Kelvin images as the negative vacancies at the steps inside the NaCl regions. This does not change when the surface is reconstructed by annealing (see next Section). It therefore seems that the Suzuki surface also has a Debye-Frenkel layer (see Sect. 15.2), which formation, structure and function remains unknown so far.

15.3.2.2 Surfaces Modified by Diffusion and Evaporation

If *pure alkali halides* like NaCl are annealed in vacuum at temperatures between 200 and 260 °C the mobility of surface ions is already large enough to significantly change the surface morphology (surface diffusion) [9]. At temperatures higher than ∼260 °C the surface starts to evaporate [8, 130] (surface evaporation) creating well-documented surface evaporation patterns [8, 131].

Quite similar diffusion and evaporation phenomena appear also on the surfaces of *doped alkali halides*. With respect to divalent metal impurity cations, the impurities even decrease the evaporation rate and increase the activation energy of evaporation [132]. Furthermore, a segregation of impurities from the bulk to the surface can have a significant impact onto the surface morphology [133]. For instance, if a NaCl crystal with a relatively large amount of Cd^{2+} (e.g., 4 Mol % $CdCl_2$) is annealed at temperatures around 250 °C the surface diffusion dramatically changes the almost quadratic shape found on as-cleaved surfaces to a more round one [126] (Fig. 15.4a, b). For relatively low impurity concentrations the shape of the Suzuki regions is again almost square-like after annealing (see below), however, the size of the regions is much smaller in comparison to the one of the large, square shaped regions on as-cleaved surfaces (Fig. 15.4c, d)—a signature for a strong diffusion that takes place also on those surfaces.

The size and number of Suzuki precipitates depend on the annealing time [10], the speed of the cooling [11] and the nominal impurity content inside the crystal [12], whereas the location of the regions depends on the step density [22, 126]: Suzuki regions can always be found on the top side of steps where they form a fringe and follow a characteristic zig-zag shape of the steps (Fig. 15.4c, d). The lower terrace is mostly a pure NaCl one (for low impurity concentrations). Interestingly, the steps do not have anymore the preferred ⟨001⟩ surface direction of non-polar steps, which can be observed on pure NaCl(001) surfaces. They run along equivalent ⟨011⟩ directions implying that they are possibly polar steps (Fig. 15.5a). If the step density is relatively low and the terrace width wider than 150–200 nm rectangular Suzuki regions can

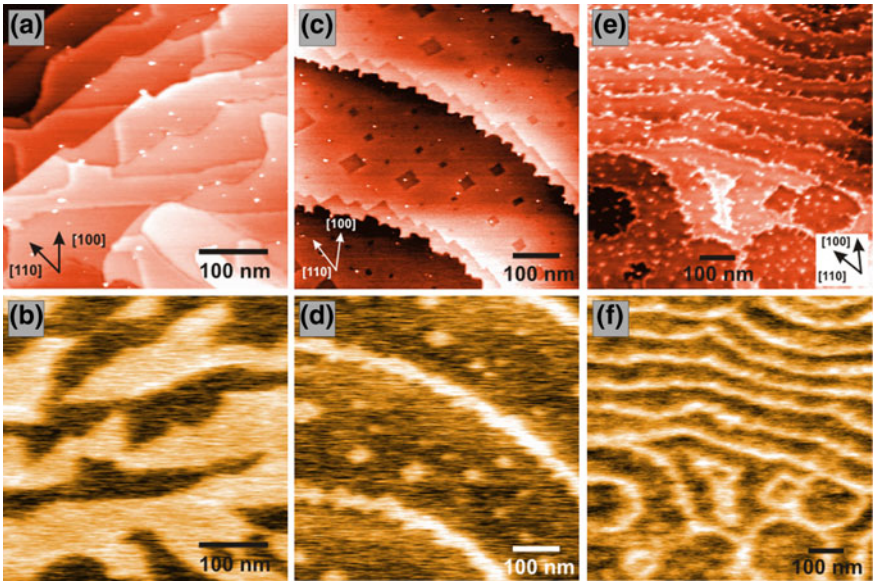

Fig. 15.4 NaCl:Cd^{2+}(001) Suzuki surfaces prepared by UHV cleavage and additional annealing. Shown are surfaces, which were influenced by surface diffusion (**a**) to (**d**) and surface evaporation (**e**) and (**f**). Crystals with a high concentration of impurities exhibit large Suzuki regions **a** and **b** whereas low impurity concentrations lead to smaller regions **c** and **d**. On evaporated surfaces, Suzuki regions can only be found at steps **e** and **f**. Shown are topography images **a**, **c**, **e** and simultaneously recorded Kelvin images **b**, **d** and **f**. Sample preparations: 4 Mol % $CdCl_2$, annealing: T = 230 °C for 5 h **a** and **b**, 1 Mol % $CdCl_2$, annealing: T = 205 °C for 5 h **c** and **d** and 2 Mol % $CdCl_2$, annealing: 340 °C for 35 min (**e**, **f**) (From [126])

also be found on the flat terraces (Fig. 15.4c, d). Obviously, the formation of Suzuki regions at steps is energetically more favorable in comparison to Suzuki regions on the flat terraces.

Very important characteristics of annealed Suzuki surfaces in general are the flatness of the Suzuki regions, the relative height between Suzuki and pure NaCl regions and the interface Suzuki-NaCl [22, 126]: all Suzuki regions are free of steps, which is a signature that, in equilibrium, a Suzuki region prefers an atomically flat surface (see all topography images in Fig. 15.4). Furthermore, both regions are almost on the same height, as it can be observed by atomic resolution imaging at the interface Suzuki-NaCl on the terraces (Fig. 15.5b). In other words, the Suzuki regions are perfectly embedded into the NaCl regions. Last, the interface between the two regions, which always runs along equivalent ⟨001⟩ surface directions, is well-defined at the atomic scale and only measures a few Ångströms (Fig. 15.5b).

When doped crystals are annealed at much higher temperatures (>300 °C), the surface starts to evaporate (surface evaporation) as on the surfaces of pure NaCl [8], in particular at steps and dislocations (Fig. 15.4e, f). In the case of NaCl:Cd^{2+}, the surface is basically comparable to an evaporated surface of pure NaCl, despite a mod-

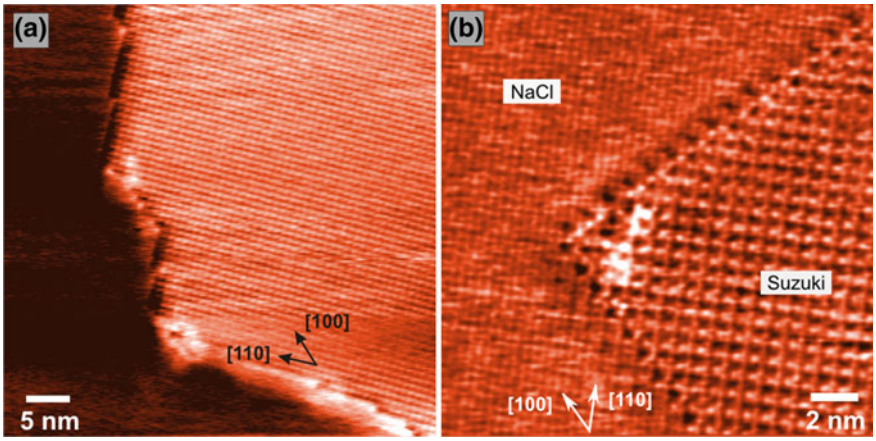

Fig. 15.5 Steps on the Suzuki surface and the interface NaCl-Suzuki on the flat terraces. **a** Constant height image representing a mono-atomic high step ($h = a_{\mathrm{NaCl}}/2$) in atomic resolution. The upper terrace is a Suzuki region, on which the lattice of either the vacancies or the Cd^{2+} ions is visible. Such steps always have a $\langle 011 \rangle$ orientation. **b** Constant height image which shows that the interface formed by the two regions, pure NaCl and Suzuki, is well-defined at the atomic scale. Either the sub-lattice of the vacancies or the Cd^{2+} ions were imaged in Suzuki regions whereas in regions of NaCl either the sub-lattice of the Na^{+}or Cl^{-} ions can be seen **b**. Both images: a dark contrast belongs to more positive detuning values and vice-versa (From [126] **a** and [40] **b**)

ification of the steps by Suzuki regions [126]: for instance, the topography image in Fig. 15.4 e shows curved (top) and circular (bottom) mono-atomic high steps ($h = a_{\mathrm{NaCl}}/2$) forming disc-shaped terraces (bottom). Such evaporation features are comparable to those ones observed on the surfaces of pure NaCl at similar temperatures [8]. However, the steps are not as smooth as on the latter surfaces [8, 131], the steps exhibit rather a zig-zag shape, which is curved on a larger scale forming the disc-shaped holes. Also here, the steps are oriented along equivalent $\langle 110 \rangle$ surface directions whereas the borders of embedded Suzuki regions point along equivalent $\langle 100 \rangle$ surface directions. A striking observation is that on wide terraces no Suzuki regions can be found despite some small pits. The pits are probably a signature that Suzuki regions on terraces are additional surface sites from where evaporation takes place. If so, such regions on the terraces disappear during the evaporation process.

15.3.3 Atomic Resolution and Identification

Atomic resolution imaging on alkali halide surfaces has become nowadays a standard, and all mechanisms of the atomic contrast formation are almost fully understood [134]. Although all atoms in the tip and surface but also tip- and surface-atom relaxations have to be taken into account, one can roughly simplify the contrast formation by considering a single atom at the apex interacting with a single atom in the surface.

For ionic surfaces like NaCl(001) and for ionic tips, the electrostatic potential of the tips' last atom determines the atomic contrast: a cation at the tip apex (e.g., Na^+ ion at the tip) images the Cl^- ions as bright ions due to an attractive force between both, and the Na^+ ions as dark ions (repulsive interaction). Vice-versa, an anion at the tip (e.g., Cl^- ion) images the Na^+ and Cl^- ions as bright and dark ions, respectively—the contrast gets basically reversed when the cation at the tip is replaced with an anion. This contrast formation has been further benchmarked on the Suzuki surface because of its interesting properties (see Sect. 15.3.1): the atomic structure is composed by three different types of ions and additional cation vacancies. Furthermore, it has four sub-lattices, which differ in their dimension and orientation, and last but not least relaxations of some ions of the surface upon tip approach may sensitively influence the contrast formation.

In the following, we qualitatively describe the contrast formation inside the Suzuki regions: when imaging with atomic resolution a regular structure composed of different bright and dark ions is regularly observed (Fig. 15.6), which can vary from surface to surface but also from tip to tip. Figure 15.6a shows an image, which was obtained on a Suzuki terminated NaCl:Mg^{2+}(001) surface (dark contrast: stronger interaction and vice-versa): dark spots (e.g., at position 1) can be seen but also additional bright spots (e.g., at position 2) forming a sub-lattice, which is parallel to the

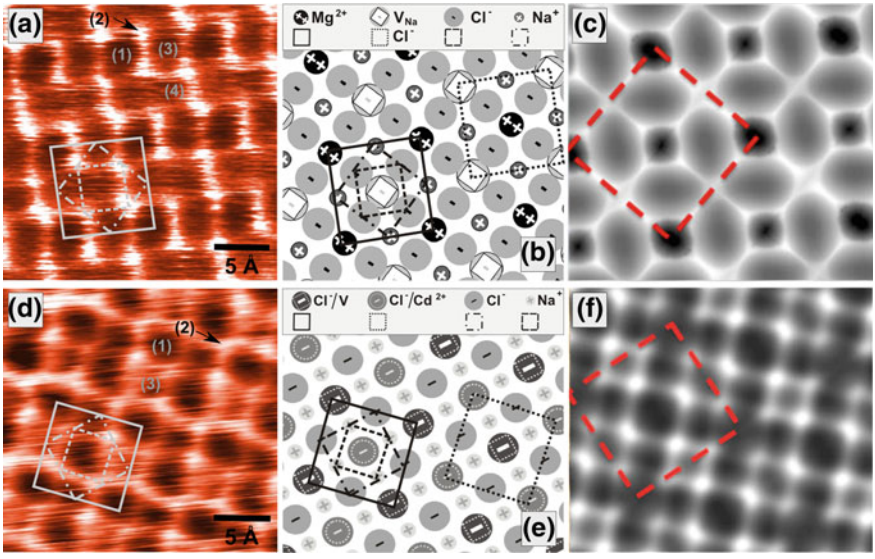

Fig. 15.6 Atomic resolution imaging on the Suzuki surface and identification of ions. Images **a** and **d** are experimental detuning images obtained in the constant height mode on a Suzuki terminated NaCl:Mg^{2+}(001) and NaCl terminated NaCl:Cd^{2+}(001) surface, respectively. Both images represent the ions and vacancies drawn in panel (**b**) and (**d**). Images **c** and **f** are simulated images, which best represent the contrast in image **a** and **c**, respectively. They were calculated with an anion (**c**) and cation terminated tip (**f**). The *red squares* mark the projected unit cell of the Suzuki structure on the (001) surface (**c**) and (**f**) (From [22] (**a**), (**b**) and [25] (**c**) to (**f**))

one of the dark spots but half as large. The dimension of the latter lattice coincides with the smallest possible sub-lattice of the Suzuki phase formed by the Cl^- ions so that the bright ions (2) can be assigned to the Cl^- ions (compare with drawing in Fig. 15.6b). This has the important consequence, that the tip's last atom obviously had a negative potential producing a repulsive interaction with the Cl^- ions. With this the divalent positive Mg^{2+} and Na^+ ions should be imaged in a darker contrast. And indeed, the darkest spots (1) belong to the Mg^{2+} ions because they exhibit a stronger interaction with the tip than the Na^+ ions. The latter Na^+ ions are always in between two dark Mg^{2+} ions (3) with a less darker contrast but also less brighter contrast than the Cl^- ions. As expected, the quadratic sub-lattice of the Na^+ ions is smaller than the Mg^{2+} lattice but larger than the Cl^- one and rotated by 45° with respect to the Cl^- and Mg^{2+} lattices. Last, the vacancies are located in the middle of a Mg^{2+} square, where also a gray contrast can be found (4) in the experimental image.

The latter qualitative description of the contrast formation has been fully supported by a comparison between experiment and Density Functional Theory (DFT) calculations [25] (Fig. 15.6c). Same calculations also simulated the atomic contrast for a cation terminated tip, which is clearly different in comparison to the contrast explained above. A very important result from theory is, that relaxations of surface ions upon an approach of the tip play a fundamental role (Fig. 15.7): when the tip is relatively far away (Fig. 15.7a), the Na^+ ions displace towards the tip's last atom, which has a negative potential as described above. This increases the contrast at the Na^+ being almost comparable to the one of the Mg^{2+} ions despite having only half the charge of the Mg^{2+} ions. The result is that the Na^+ ions produce a similar contrast as the Mg^{2+} ions. However, when the tip comes relatively close to the surface (Fig. 15.7b, c) the interaction with the Mg^{2+} ions becomes dominant so that the Mg^{2+} ions create the strongest contrast in the images.

So far, we have considered the Suzuki termination only. With respect to the NaCl termination similar mechanisms could be observed [25]: Fig. 15.6d shows the contrast of an experimental image of a NaCl:Cd^{2+}(001) Suzuki surface: the contrast is formed by large dark spots (1), which form a sub-lattice equal to the one formed by either the Cd^{2+} ions or the Na^+ vacancies (compare with drawing in Fig. 15.6e). Four bright spots can be found (2) around each dark spot forming a sub-lattice of either Cl^- or Na^+ ions, and some additional less dark spots are in between the large dark spots. Calculations on the *Suzuki terminated* surface were unable to reproduce the observed contrast with any type of tip (anion or cation terminated tip, Fig. 15.7d). Only the *NaCl terminated surface* was able to best reproduce the experimental image with a cation terminated tip (Fig. 15.6f), demonstrating that, in this case, the NaCl:Cd^{2+} Suzuki region most likely had an NaCl termination.

With respect to the development of contrast upon tip approach, atomic displacements play again a fundamental role (Fig. 15.7e, f): in the absence of the tip, the Cl^- ions over vacancies displace strongly outwards from the surface (0.04 nm, Fig. 15.7e), while those over Cd^{2+} remain close to the ideal surface plane. This results in a strong contrast of the Cl^- ions above the second-layer vacancies at long tip-surface distances, strongly enhanced due to large tip-induced displacements of such Cl^- ions.

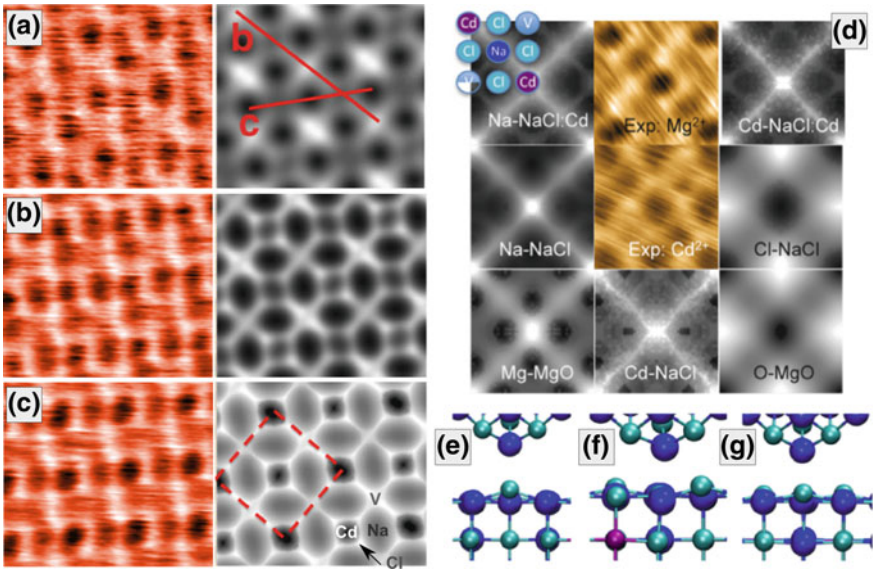

Fig. 15.7 The contrast formation in atomic resolution imaging. **a–c** Comparison of experimental (*left*) and simulated data (*right*) for NaCl:Mg^{2+}. The simulations used a Cl-terminated NaCl tip. The experimental images corresponds to average detuning values of −16, −22 and −24 Hz (*top-bottom*, with a more negative detuning corresponding to imaging closer to the surface). The simulated data corresponds to tip-surface *heights* of 0.45, 0.325 and 0.275 nm, resulting in average detunings of −16.4, −21.8 and −23.0 Hz, respectively. **d** Comparison of experimental images of NaCl:Mg^{2+} and NaCl:Cd^{2+} with simulated images of NaCl:Cd^{2+} (Suzuki termination) using seven different tips X:Y (*gray scale*), where Y is the tip material and X is the terminating atom. None of the 7 images reproduces the contrast of the experimental image in the middle (NaCl:Cd^{2+}). **e–g** Simulation snapshots showing key atomic displacements for a Na-terminated NaCl tip imaging NaCl:Cd^{2+} (NaCl termination) at a tip height of **e** 0.46 nm over a Cl^- site above a vacancy, **f** 0.31 nm over an Na^+ site, and **g** 0.4 nm over a Cl^- site above a Na^+ (From [25])

At close distance, a reduction in repulsion over Na^+ ions due to displacements of neighboring Cl^- ions towards the tip can be observed. Furthermore, the attractive interaction to the rigidly held Cl^- ions above the second-layer Cd^{2+} ions and of the Cl^- ions above the second-layer Na^+ ions increases, also partially due to displacements of the Cl^- ions towards the tip. All this results into an image as shown in Fig. 15.6d where the Cl^- ions above the vacancies still exhibit the strongest contrast, which is, however, comparable to the contrast of Cl^- ions above the Cd^{2+} and Na^+ ions.

The extensive comparison between experiment and theory in [25] shows that the identification of all ions and the vacancies can be done independently of the tip-surface distance, of the chemical nature of the divalent impurity ions inside the Suzuki structure, and despite differences in surface termination. Therefore, with an image library at hand (see Supporting Information of [25]), which shows the atomic contrast for both surface terminations and both types of tips (anion and cation terminated),

all ions in the Suzuki structure can be identified by just atomic resolution imaging, thereby providing characterization of the tip's potential. This identification is possible due to the doping of NaCl with divalent impurity ions and thanks to the geometry of the atomic Suzuki structure, which contrasts the situation on the pure NaCl(001) surface where such chemical identification is not possible. Important to note is that the development of contrast patterns as a function of tip-surface separation is strongly linked to tip-induced atomic displacements, which is significantly different to the contrast formation on the surfaces of pure alkali halides.

Several other Suzuki systems in NaCl exist, including the magnetic impurities Mn^{2+} and Fe^{2+} [10], which probably form an antiferromagnetic ordering [25]. This might be particularly interesting for exchange force microscopy, which could resolve different spin orientations [135]. Other types of host system for the Suzuki phases are oxides like MgO:Mn^{4+} [117] and NiO:Mn^{4+} [120], which could be used as substrates in heterogeneous model catalysis. In general, doping of insulators, in combination with high resolution nc-AFM, provides a general tool for characterizing surfaces at the atomic scale. For instance, the wide use of doping with impurities of different valences in many insulators such as ZrO_2 and CeO_2 [136, 137] suggests that the method could also be used in high resolution studies of their surfaces.

15.4 Supported Nano-objects on the Suzuki Surface

The rediscovery of the nanostructured Suzuki surface by nc-AFM and KPFM is quite promising for applications in nanosciences because of the specific Suzuki structure but also because of the two distinct surface regions that co-exist at the same time. In particular for investigations of deposited molecules and metal NPs the Suzuki surface is an attractive choice. And indeed, as summarized and discussed in the following two sections recent work has shown that metal nanoparticles or molecules exhibit interesting growth modes, which are different in both surface regions and which can only appear on the Suzuki surface at the same time [40, 41].

15.4.1 Metal Nanoparticles

The growth and characterization of metal nanoparticles (NPs) on oxide and similar surfaces is of large interest in heterogeneous model catalysis because the morphology (size and shape), distribution and electronic properties of NPs determine if the rate of a catalytic reaction is increased by the catalysts or not [138, 139]. A very important objective for reactivity measurements, which measure over large surface areas (like molecular beam or temperature programmed desorption experiments), is that the NPs have all the same size and shape: this allows assigning specific properties of a reaction to one type of NP, and by varying the size, shape and composition of the NPs the reaction can be characterized [140]. A narrow size distribution of equally shaped NPs

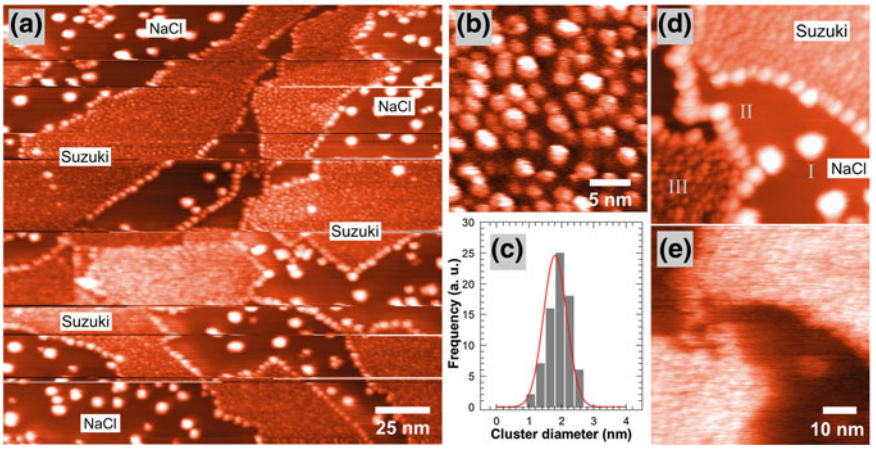

Fig. 15.8 The confined growth of PdNPs in Suzuki regions (quantity: 0.35 mono-layers of Pd, growth at room temperature). **a** Large-scale topography image after the deposition (each *bright dot* is a single NP). Palladium forms NPs preferentially in the Suzuki regions. **b** Constant height image obtained inside a Suzuki region and histogram (**c**) of the NP sizes found from image (**b**). Topography (**d**) and Kelvin image (**e**) obtained in one KPFM measurement. The Kelvin image exhibits large voltage differences between the stoichiometric NaCl terraces and the NPs inside the Suzuki regions (Kelvin contrast: $U_{PdNPs-Suzuki} = +3$ to $+4$ V) (From [40])

can be obtained on nanostructured surfaces, which exhibit an ordered arrangement of defects like on the nanostructured alumina film on $Ni_3Al(111)$ [141]. Therefore, after the rediscovery of the nanostructured Suzuki surface it was promising to test if also on this surface metal NPs can be grown into an ordered NP assembly, with a small NP size distribution inside the Suzuki regions. A recent work considered palladium nanoparticles on the NaCl:Cd^{2+} Suzuki surface, on which we will focus in the following [40].

If Pd atoms are deposited on the (001) surfaces of *pure NaCl* (sample at room temperature) they diffuse on the terraces. Because of the specific kinetics at room temperature the nucleation at steps is faster than on terraces [138] so that Pd preferentially forms nanometer sized NPs decorating the steps [142, 143]. Almost no stable NPs can be found on the terraces. On the contrary, depositing Pd on a *Suzuki surface* results into a completely different surface, which is characterized by three different types of NPs (Fig. 15.8a, d). The first type of NP (I) can be found occasionally on the flat terraces of pure NaCl. Due to the low defect density in these regions, the NPs, once formed, collect a large part of Pd atoms diffusing on the pure NaCl terraces, so that the NPs become quite large (height $h_I = 2.4$ nm, diameter $D_I = 3$–4 nm) [138]. The second type of NP (II) is located at the NaCl-Suzuki boundary where the NP collects obviously less Pd—this can be seen by the smaller size of the nanoparticles ($h_{II} = 1.5$ nm, $D_{II} = 2.5$ nm).

A different situation can be found inside the Suzuki regions, where the PdNPs (III) are much smaller and the NP density much higher (Fig. 15.8b). The density

($\rho_{\text{Suzuki}} \approx 1.3 \times 10^{13}$ NPs/cm^2) is more than forty times higher with respect to the density in the pure NaCl regions ($\rho_{\text{NaCl}} \approx 3 \times 10^{11}$ NPs/cm^2). Each NP divides the surface on a circular surface area with a radius of 1.6 nm and has therefore a mean distance of about 3 nm to their neighboring NPs, which is four times larger than the size of the largest sub-lattice formed by either the Cd^{2+} impurity ions or the vacancies ($a_{V,Cd^{2+}} \approx 0.8$ nm, see Fig. 15.2). Due to the high density of nucleation sites, each NP collects much less Pd during the metal deposition than the NPs in the pure NaCl regions, which explains the quite small size of the NPs: the almost round NPs have a very small diameter, but also a very small height that corresponds to only a few atomic layers ($h_{\text{III}} = 0.6 \pm 0.2$ nm, $D_{\text{III}} = 1.8 \pm 0.4$ nm). Due to the different sizes of the three type of NPs, a NP in the Suzuki region has roughly ~50 atoms, whereas a much larger number of atoms can be found in a NP at the NaCl-Suzuki interface (~400 atoms) and especially in a NP that is located somewhere on the flat NaCl terrace (~1500 atoms).

It is obvious that the specific ionic structure of the Suzuki phase plays a key role in the nucleation of the NPs. An interesting conclusion can be drawn when considering the ratio height-to-diameter: The value is almost the same for the NPs in the NaCl regions and at the interface Suzuki-NaCl ($h_{\text{I}}/D_{\text{I}} = 0.68 \approx h_{\text{II}}/D_{\text{II}} = 0.6$), but two times larger than the value of the NPs inside the Suzuki regions ($h_{\text{III}}/D_{\text{III}} = 0.33$). This is directly related to the adhesion energy E_a: the flatter a NP is, the larger is the substrate-NP interaction [138]. Therefore, the nanoparticle-surface interaction must be stronger inside the Suzuki regions than in the NaCl regions. Since metal especially likes electronegative surface sites [43, 144], potential candidates that can exhibit a strong interaction with the NPs are the negative vacancies on Suzuki terminated surfaces or, on NaCl terminated surfaces, the chlorine ions above the vacancies (Cl_V^-). First principles calculations predict indeed that atomic Pd prefers to adsorb in Suzuki regions by up to 0.4 eV over the ideal NaCl surface with the favored sites of Cl_V^- for the NaCl termination and the vacancies and Cl^- ions for Suzuki termination.

Surprisingly, from the experiments it can be found that not all of these sites are occupied by NPs. Only every ~12th surface site is occupied, which again could be due to kinetics [138], but also due to repulsive forces amongst NPs. It has been shown that NPs may repel each other if elastic forces caused by strain fields in the NP-substrate interface [145] or repulsive electrostatic forces amongst charged NPs occur [146]. The latter repulsive electrostatic interaction amongst NPs seems to be reasonable: because a NP can cover several of equivalent surface sites like vacancies on the Suzuki terminated surface, large polarization or charge effects can be expected. Indeed, Kelvin images show a very bright contrast at the NPs inside the Suzuki regions with respect to the neutral and stoichiometric NaCl regions, which appear dark in the Kelvin images (Fig. 15.8e). The change of contrast from bright to dark corresponds to voltage differences of several volts, which can be sometimes as large as 4 V. These values are much larger than the voltage difference between clean Suzuki and NaCl regions that have been ever measured [126] (see Sect. 15.3.2.1 and 15.3.2.2). In comparison to the small NPs in the Suzuki regions, the large NPs in the pure NaCl regions exhibit a less bright contrast (Kelvin contrast: ~1.5 V), which is because such NPs probably cover only a single vacancy. The Kelvin images therefore

confirm a charging/polarization of NPs inside the Suzuki regions, which explains in turn possible repulsive electrostatic forces amongst the NPs as discussed above.

In conclusion, a narrow size distribution of very small, nanometer sized PdNPs can be obtained on the Suzuki surface unlike on the surfaces of pure alkali halides. This is thanks to the selective growth of palladium inside the Suzuki regions and the specific structure of the Suzuki phase. The work motivates studying the detailed growth of any kind of NP as a function of NP material (one and two componant NPs like bi-metallic NPs), NP quantity and growth temperature. The small nanometer size and narrow size distribution is ideal for reactivity measurements, which measure over large surface areas, but also for nc-AFM and KPFM that can contribute to reactivity studies as exemplified by a recent KPFM work on PdNPs on graphite [147]. Although the Suzuki surface is not relevant in heterogeneous catalysis adsorption, desorption and reactivity related phenomena at NPs could yield suitable information at, at least, low temperatures ($<100\,^{\circ}\mathrm{C}$).

15.4.2 Functionalized Molecules

In recent years, it has been discussed how small molecules adsorb on ionic insulating surfaces [31, 37, 40, 148, 149] and which impact the adsorption has on the self-assembly of molecules [150]. A common finding is that the adsorption of, e.g., non-polar molecules is relatively weak due to van der Waals forces, which are not strongly site specific—the molecules can occupy almost any position on the surface [30]. However, as soon as a molecule includes atoms carrying a partial charge or polar groups, the polar groups of the molecule can directly bind to the ionic surface lattice via an electrostatic interaction (*charge matching*) [31, 37, 40, 148, 149].

Because the Suzuki surface exhibits two distinct surface regions (pure NaCl and Suzuki regions) which differ in their atomic structure (e.g., see Sect. 15.3.2 and 15.3.3), it is quite appealing to study phenomena of adsorption and self-assembly as a function of surface site to shed more light onto the detailed mechanisms involved. Recently, the adsorption and self-assembly of four functionalized pentahelicene molecules ([5]helicene, neutral molecule: $C_{22}H_{14}$) (Fig. 15.9a) have been studied as a function of adsorption geometry and dipole strength on the Suzuki surface [40, 41]. The molecules were functionalized either with one or two bromine substituents or cyano substituents (MonoBromo, DiBromo, MonoCyano and DiCyano) substituting regular hydrogens at positions 6 and 7 of the molecules (racemic samples). The molecules differ in their dipole strength (from MonoBromo to DiCyano: -1.92, -2.88, -5.76 and -9.27 Debye) but also in the geometry if two substituents are attached to the molecule (distance d of substituents: 0.34 nm (DiBromo) and 0.41 nm (DiCyano, N–N)).

Experiments with MonoBromo have shown that it only adsorbs at defects of the NaCl surface, which can be best observed on the surfaces of *pure NaCl crystals* [40]: the molecules stick exclusively at the steps and form molecular wires. The whole adsorption changes, if MonoBromo is deposited onto the *Suzuki surface* (Fig. 15.9b): the molecules cover all Suzuki regions by forming flat homogeneous islands, and

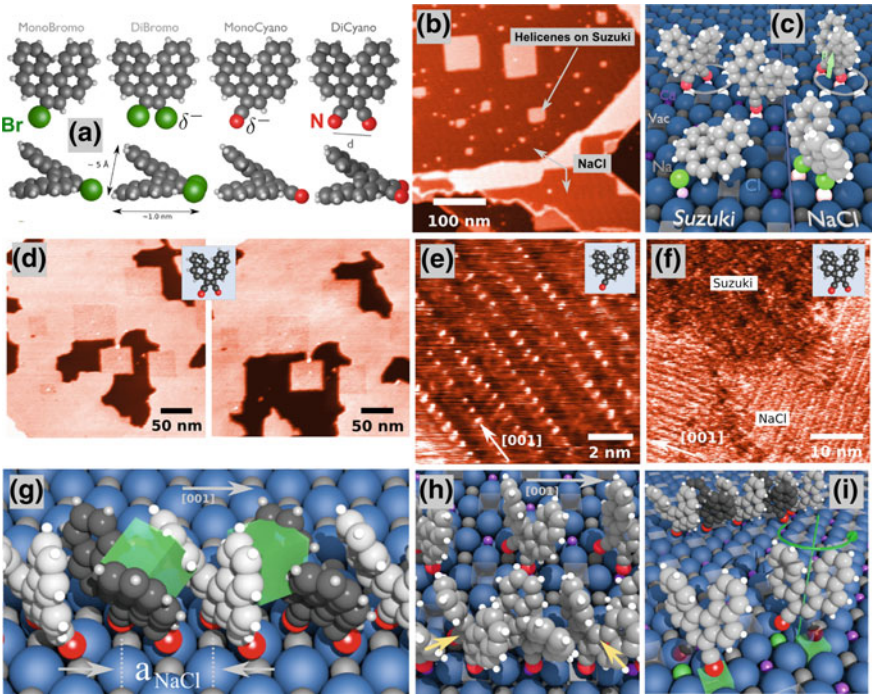

Fig. 15.9 Functionalized [5]helicene molecules on the NaCl:Cd^{2+}(001) surface **a** MonoBromo, DiBromo, MonoCyano and DiCyano. **b** A single molecular layer of MonoBromo perfectly decorates all Suzuki regions. **c** Model of adsorption based on the charge-matching principle. **d** The desorption of DiCyano from regions of pure NaCl (3.4 h distance between images). **e** Self-assembly in one molecular layer of MonoCyano inside a Suzuki region. Each *bright spot* is a single molecule. **f** DiCyano inside a Suzuki (amorphous) and NaCl region (self-assembled). **g** Result from theory showing the π-π stacking of DiCyano along ⟨001⟩ surface directions. Both enantiomers are alternately placed along the row. The *green box* has a dimension of 3.5 Å symbolizing the typical π-π bonding distance. **h** Half of the DiCyano molecules are placed above the negative vacancies of the Suzuki surface (*bottom row*, *yellow arrows*), they need to be removed (*top row*). **i** By turning MonoCyano around its long axis (*bottom*) the single cyano group can always be positioned above a cation such that self-assembly becomes possible in the Suzuki regions as exemplified by the *top row* of molecules (From [40] (**b**) and [41] (**a**, **c**) to (**i**))

no molecule is located in the NaCl regions. Due to the two-dimensional shape of the Suzuki regions and the well-defined NaCl-Suzuki interface the monolayer high islands have exactly the same shape and size as the Suzuki regions. A comparison between experiment and theory has shown that the molecules are lying flat on the surface such that the bromine atom with its partial negative charge is charge-matched at a cation (bottom left molecule in Fig. 15.9c). Two-thirds of the adsorption energy ($\overline{E}_{ad} \approx 0.87$ eV [1]) stems from a van der Waals contribution between the surface and

[1]The adsorption energy $\overline{E}_{ad}$ is an average value of the two adsorption energies obtained on the Suzuki and NaCl terminated surface.

the closest benzene rings, and one third is due to an electrostatic interaction between the bromine atom and the cation, which pins MonoBromo on the surface.

In contrast to MonoBromo, which remains on the surface for all time after its deposition, all other three [5]helicene molecules desorb within hours days and weeks from the surface as a function of their dipole strength (see desorption of DiCyano in (Fig. 15.9d). Furthermore, they are all standing perpendicular on the surface, in contrast to MonoBromo. An analysis of all the experimental data and assisting theory developed a conclusive model of adsorption (Fig. 15.9c): MonoBromo adsorbs in a flat configuration (see above) whereas DiBromo stands perpendicular on the surface (bottom right molecule in (Fig. 15.9c). However, DiBromo desorbs within hours due to its very small dipole and the resulting small coupling to the cations, the mismatch between the two bromines and the surface cations and the missing van der Waals interaction ($\overline{E}_{\mathrm{ad}} \approx 0.23$ eV). Both cyanated molecules are also in a perpendicular position (top molecules in (Fig. 15.9c), with their negative cyano substituents charge-matched at the cations. Due to their strong dipole, the adsorption energy is considerably larger in comparison to the one of DiBromo but smaller than the one of the flat lying MonoBromo (MonoCyano: $\overline{E}_{\mathrm{ad}} \approx 0.50$ eV, DiCyano: $\overline{E}_{\mathrm{ad}} \approx 0.74$ eV). In particular the two cyano groups of DiCyano perfectly match with two cations (distance $d_{\mathrm{Na–Na}} = d_{\mathrm{Na–Cd}} = 0.40$ nm) resulting into a strong interaction. All this explains why both cyanated molecules remain for a relatively long time of ∼2 weeks on the surface.

Both cyanated [5]helicene molecules form self-assembled molecular rows along the $\langle 001 \rangle_{\mathrm{NaCl}}$ surface direction (Fig. 15.9e, f). A major observation is that MonoCyano self-assembles in the Suzuki regions and probably also in the NaCl regions, which could not be verified due to the weak adsorption of the molecules—the molecules desorbed from the surface under the influence of the AFM tip. In contrast, DiCyano only self-assembles in the NaCl regions of the Suzuki surface but not inside the Suzuki regions, in which only an amorphous structure of DiCyano could be observed. Thanks to the combination of experiment and theory it could be shown that the molecules have a distance of the NaCl unit cell (0.564 nm) along the $\langle 001 \rangle_{\mathrm{NaCl}}$ direction, which permits a π-π stacking of adjacent benzenoid rings of the helicene molecules, with a typical bonding distance in the order of ∼3.5 Å (Fig. 15.9g). The stacking of molecules increases the total energy of the system by 0.2 eV/molecule, which is also one of the reason why the molecules are in a perpendicular position on the surface. With respect to DiCyano, a molecular row placed inside the Suzuki regions positions the substituents of half of the molecules above the negative vacancies of the Suzuki surface (bottom row in Fig. 15.9h). In this case, the adsorption is very small ($\triangle E_{\mathrm{ad}} = 0.18$ eV) so that half of the molecules need to be removed destroying the self-assembly (top row in Fig. 15.9h), which explains the amorphous structure observed in experiments. In contrast, MonoCyano can self-assemble in the Suzuki regions (top row in Fig. 15.9i) since the single substituent can always be positioned above a cation by a rotation of the molecule along its long axis, which stands perpendicular on the surface (bottom in Fig. 15.9i).

In summary, the mechanisms of adsorption and self-assembly of functionalized helicene molecules can be studied in great detail on the Suzuki surface, which is

thanks to the two distinct surface regions and the specific atomic structure of the Suzuki surface. The rule of thumbs for the adsorption and self-assembly might help to predict the adsorption and self-assembly of other helicene molecules, e.g., helicene molecules functionalized with three substitutents. By meeting the charge matching criteria, such molecules probably bind more selectively in a flat and stable position such that flat molecular templates can be created, which is interesting for chiral recognition and templating applications. It is clear that in general, the Suzuki surface is attractive also for many other molecules, opening promising perspectives in the domain of self-assembled molecules on insulating surfaces.

Acknowledgments The author expresses his great appreciation to A. S. Foster, T. Hynninen, C. R. Henry, B. Hoff, and in particular to A. L. Shluger and S. Gauthier for stimulating discussions. The author acknowledges the European Science Foundation for financial support through the FANAS project NOMCIS and the French agency for Research (*Agence Nationale pour la Recherche*, ANR) for financial support through the programs CANA and MISS. Support by the European COST through action D41 is highly acknowledged.

References

1. W. Hayes, A.M. Stoneham (eds.), *Defects and Defect Processes in Nonmetallic Solids* (Wiley-Interscience, New York, 1985)
2. F. Seitz, Rev. Mod. Phys. **18**, 384 (1946)
3. F. Seitz, Rev. Mod. Phys. **26**, 7 (1954)
4. G. Binnig, C.F. Quate, Ch. Gerber, Phys. Rev. Lett. **56**, 930 (1986)
5. G.A. Bassett, Philos. Mag. **3**, 1042 (1958)
6. H. Bethge, J. Heydenreich (eds.), *Elektronenmikroskopie in der Festkörperphysik* (Springer, Berlin, 1982)
7. H. Bethge, Surf. Sci. **3**, 33 (1964)
8. H. Bethge, K.W. Keller, J. Cryst. Growth **23**, 105 (1974)
9. H. Höche, H. Bethge, J. Cryst. Growth **33**, 246 (1976)
10. G.A. Bassett, M.J. Yacamán, Thin Solid Films **31**, 375 (1976)
11. M.J. Yacamán, J.P. Hirth, Thin Solid Films **38**, 215 (1976)
12. G. Grange, Surf. Sci. **105**, 265 (1981)
13. T.R. Albrecht, P. Grütter, D. Horne, D. Rugar, J. Appl. Phys. **69**, 668 (1991)
14. S. Morita, R. Wiesendanger, E. Meyer (eds.), *Noncontact Atomic Force Microscopy* (Springer-Verlag, Berlin, 2002)
15. F.J. Giessibl, Rev. Mod. Phys. **75**, 949 (2003)
16. C. Barth, A.S. Foster, C.R. Henry, A.L. Shluger, Adv. Mater. **23**, 477 (2011)
17. M. Bammerlin, R. Lüthi, E. Meyer, A. Baratoff, J. Lü, M. Guggisberg, C. Loppacher, C. Gerber, H.-J. Güntherodt, Appl. Phys. A **66**, S293 (1998)
18. R. Bennewitz, S. Schär, E. Gnecco, O. Pfeiffer, M. Bammerlin, E. Meyer, Appl. Phys. A **78**, 837 (2004)
19. R. Hoffmann, L.N. Kantorovich, A. Baratoff, H.-J. Hug, H.-J. Güntherodt, Phys. Rev. Lett. **92**, 146103 (2004)
20. S.A. Burke, J.M. Mativetsky, R. Hoffmann, P. Grütter, Phys. Rev. Lett. **94**, 96102 (2005)
21. A. Schirmeisen, D. Weiner, H. Fuchs, Phys. Rev. Lett. **97**, 136101 (2006)
22. C. Barth, C.R. Henry, Phys. Rev. Lett. **100**, 096101 (2008)
23. K. Ruschmeier, A. Schirmeisen, R. Hoffmann, Phys. Rev. Lett. **101**, 1 (2008)

24. M.A. Cerda, J. Abad, A. Madgavkar, D. Martrou, S. Gauthier, Nanotechnology **19**, 045503 (2008)
25. A.S. Foster, C. Barth, C.R. Henry, Phys. Rev. Lett. **102**, 256103 (2009)
26. C. Barth, C.R. Henry, Phys. Rev. Lett. **98**, 136804 (2007)
27. P. Egberts, T. Filleter, R. Bennewitz, Nanotechnology **20**, 264005 (2009)
28. A. Hinaut, Dissertation, Université Toulouse III Paul Sabatier, 2012
29. T. Filleter, S. Maier, R. Bennewitz, Phys. Rev. B **73**, 1 (2006)
30. O.H. Pakarinen, J.M. Mativetsky, A. Gulans, M.J. Puska, A.S. Foster, P. Grütter, Phys. Rev. B **80**, 85401 (2009)
31. B. Such, T. Trevethan, T. Glatzel, S. Kawai, L. Zimmerli, E. Meyer, A.L. Shluger, C.H.M. Amijs, P. de Mendoza, A.M. Echavarren, ACS Nano **4**, 3429 (2010)
32. L. Nony, E. Gnecco, A. Baratoff, A. Alkauskas, R. Bennewitz, O. Pfeiffer, S. Maier, A. Wetzel, E. Meyer, Ch. Gerber, Nano Lett. **4**, 2185 (2004)
33. T. Kunstmann, A. Schlarb, M. Fendrich, T. Wagner, R. Möller, R. Hoffmann, Phys. Rev. B **71**, 121403 (2005)
34. T. Dienel, C. Loppacher, S.C.B. Mannsfeld, R. Forker, T. Fritz, Adv. Mater. **20**, 959 (2008)
35. S.A. Burke, W. Ji, J.M. Mativetsky, J.M. Topple, S. Fostner, H.-J. Gao, H. Guo, P. Grütter, Phys. Rev. Lett. **100**, 186104 (2008)
36. S.A. Burke, J.M. LeDue, J.M. Topple, Sh Fostner, P. Grütter, Adv. Mater. **21**, 2029 (2009)
37. A. Hinaut, A. Pujol, F. Chaumeton, D. Martrou, A. Gourdon, S. Gauthier, Beilstein J. Nanotechnol. **3**, 221 (2012)
38. L. Nony, F. Bocquet, F. Para, F. Chérioux, E. Duverger, F. Palmino, V. Luzet, C. Loppacher, Beilstein J. Nanotechnol. **3**, 285 (2012)
39. F. Bocquet, L. Nony, S.C.B. Mannsfeld, V. Oison, R. Pawlak, L. Porte, C. Loppacher, Phys. Rev. Lett. **108**, 206103 (2012)
40. C. Barth, M. Gingras, A.S. Foster, A. Gulans, G. Félix, T. Hynninen, R. Peresutti, C.R. Henry, Adv. Mater. **24**, 3228 (2012)
41. B. Hoff, M. Gingras, A.S. Foster, R. Peresutti, C.R. Henry, C. Barth, J. Phys. Chem. C **118**, 14569 (2014)
42. C. Barth, C.R. Henry, Nanotechnology **15**, 1264 (2004)
43. O.H. Pakarinen, C. Barth, A.S. Foster, C.R. Henry, Phys. Rev. B **73**, 235428 (2006)
44. C. Barth, C.R. Henry, Appl. Phys. Lett. **89**, 252119 (2006)
45. J.M. Mativetsky, S.A. Burke, S. Fostner, P. Grutter, Small **3**, 818 (2007)
46. J.M. Mativetsky, S. Fostner, S.A. Burke, P. Grutter, Phys. Rev. B **80**, 45430 (2009)
47. T. Glatzel, L. Zimmerli, S. Koch, S. Kawai, E. Meyer, Appl. Phys. Lett. **94**, 063303 (2009)
48. A. Tekiel, Y. Miyahara, J.M. Topple, P. Grütter, ACS Nano **7**, 4683 (2013)
49. L. Gross, F. Mohn, N. Moll, P. Liljeroth, G. Meyer, Science **325**, 1110 (2009)
50. L. Gross, F. Mohn, N. Moll, G. Meyer, R. Ebel, W.M. Abdel-Mageed, M. Jaspars, Nat. Chem. **2**, 821 (2010)
51. O. Guillermet, S. Gauthier, C. Joachim, P. de Mendoza, T. Lauterbach, A. Echavarren, Chem. Phys. Lett. **511**, 482 (2011)
52. L. Gross, F. Mohn, N. Moll, B. Schuler, A. Criado, E. Guitián, D. Peña, A. Gourdon, G. Meyer, Science **337**, 1326 (2012)
53. F. Mohn, B. Schuler, L. Gross, G. Meyer, Appl. Phys. Lett. **102**, 073109 (2013)
54. J. Zhang, P. Chen, B. Yuan, W. Ji, Z. Cheng, X. Qiu, Science **342**, 611 (2013)
55. C. Barth, C. Claeys, C.R. Henry, Rev. Sci. Instr. **76**, 083907 (2005)
56. C. Barth, C.R. Henry, Nanotechnology **17**, S155 (2006)
57. M. Pivetta, F. Patthey, M. Stengel, A. Baldereschi, W.D. Schneider, Phys. Rev. B **72**, 115404 (2005)
58. G. Cabailh, C.R. Henry, C. Barth, New J. Phys. **14**, 103037 (2012)
59. S. Fölsch, A. Riemann, J. Repp, G. Meyer, K.-H. Rieder, Phys. Rev. B **66**, 161409 (2002)
60. Ch. Bombis, F. Ample, J. Mielke, M. Mannsberger, C.J. Villagómez, Ch. Roth, C. Joachim, L. Grill, Phys. Rev. Lett. **104**, 185502 (2010)
61. O. Mahapatra, P.J. Kowalczyk, S.A. Brown, Surf. Sci. **620**, 45 (2014)

62. F. Golek, P. Mazur, Z. Ryszka, S. Zuber, Surf. Sci. **600**, 1689 (2006)
63. H.E. Carrillo, H.A. Carrillo, O.J. Rubio, Phys. Status Solidi **101**, 315 (1987)
64. C. Sommerhalter, T.W. Matthes, T. Glatzel, A. Jäger-Waldau, M.C. Lux-Steiner, Appl. Phys. Lett. **75**, 286 (1999)
65. T. Glatzel, S. Sadewasser, R. Shikler, Y. Rosenwaks, M.C. Lux-Steiner, Mater. Sci. Eng. B **102**, 138 (2003)
66. Y. Frenkel (ed.), *Kinetic Theory of Liquids* (The Clarendon Press, Berlin, 1946)
67. R.W. Whitworth, Adv. Phys. **24**, 203 (1975)
68. K.L. Kliewer, J.S. Koehler, Phys. Rev. **140**, A1226 (1965)
69. K.L. Kliewer, Phys. Rev. **140**, A1241 (1965)
70. K. Kliewer, J. Phys. Chem. Solids **27**, 705 (1966)
71. R.B. Poeppel, J.M. Blakely, Surf. Sci. **15**, 507 (1969)
72. M.F. Butman, A.A. Smirnov, L.S. Kudin, Z.A. Munir, Surf. Sci. **458**, 106 (2000)
73. R.C. Baetzold, Phys. Rev. B **52**, 11424 (1995)
74. J.M. Blakely, S. Danyluk, Surf. Sci. **40**, 37 (1973)
75. A.S. Foster, T. Trevethan, A.L. Shluger, Phys. Rev. B **80**, 115421 (2009)
76. H.H. Pieper, C. Barth, M. Reichling, Appl. Phys. Lett. **101**, 051601 (2012)
77. K.P. McKenna, A.L. Shluger, Nat. Mater. **7**, 859 (2008)
78. K. Suzuki, J. Phys. Soc. Jpn. **16**, 67 (1961)
79. K. Toman, Czech. J. Phys. **12**, 542 (1962)
80. D. Figueroa, E. Laredo, Solid State Commun. **11**, 1209 (1972)
81. W. Spengler, R. Kaiser, Phys. Status Solidi B **66**, 107 (1974)
82. C.J.J. Van Loon, D.J.W. Ijdo, Acta Crystallogr. B **31**, 770 (1975)
83. A. Sors, E. Lilley, Phys. Status Solidi A **32**, 533 (1975)
84. D. Figueroa, E. Laredo, M. Puma, Solid State Commun. **25**, 509 (1978)
85. N. Bonanos, E. Lilley, Mater. Res. Bull. **14**, 1609 (1979)
86. M.J. Yacamán, R.A. Gómez, J.P. Hirth, Philos. Mag. A **39**, 709 (1979)
87. N. Bonanos, E. Lilley, Solid State Ionics **1**, 223 (1980)
88. J.M. Calleja, A. Ruiz, F. Flores, V.R. Velasco, E. Lilley, J. Phys. Chem. Solids **41**, 1367 (1980)
89. A.L. Guerrero, E.P. Butler, P.L. Pratt, L.W. Hobbs, Philos. Mag. A **43**, 1359 (1981)
90. P. Aceituno, F. Cussó, A. de Andrés, F. Jaque, Solid State Commun. **49**, 209 (1984)
91. M. Chall, B. Winkler, P. Blaha, K. Schwarz, J. Phys. Chem. B **104**, 1191 (2000)
92. M. Chall, Ph.D. thesis, Kiel, Germany, 2000
93. D.L. Kirk, R.M. Innes, Thin Solid Films **28**, 243 (1975)
94. M. Yacaman, L.W. Hobbs, M.J. Goringe, Phys. Status Solidi A **39**, K85 (1977)
95. M.G. Moreno, J.C. Sal, J. Aramburu, F. Rodríguez, J.L. Tholence, F. Jaque, Phys. Rev. B **29**, 4192 (1984)
96. O.J. Rubio, F.A. Muñoz, M. Patrón, Solid State Commun. **55**, 109 (1985)
97. J.C. Gomez-Sal, M. Moreno, F. Rodríguez, A. Revex, J.L. Tholence, J. Phys. C Solid State Phys. **20**, L421 (1987)
98. J.C. Gómez Sal, F. Rodríguez, M. Moreno, J.L. Tholence, Phys. Rev. B **37**, 454 (1988)
99. F. Rodriguez, J.C. Gomez, Sal, M. Moreno, A. de Geyer, C. Janot. Phys. Rev. B **43**, 7519 (1991)
100. M.C. Marco de Lucas, F. Rodríguez, M. Moreno, Phys. Status Solidi B **184**, 247 (1994)
101. M.J. Yacamán, G.A. Bassett, J. Appl. Phys. **47**, 2313 (1975)
102. D. Barb, S. Constantinescu, S. Nistor, D. Tarinã, Hyperfine Interact. **53**, 279 (1990)
103. G. Benedek, J.M. Calleja, R. Capelletti, A. Breitschwerdt, J. Phys. Chem. Solids **45**, 741 (1984)
104. A. De Andrés, J.M. Calleja, I. Pollini, G. Benedek, J. Chem. Phys. **83**, 4967 (1985)
105. M. Hartmanova, I. Thurzo, Š. Besedičová, J. Phys. Chem. Solids **38**, 587 (1977)
106. J.E. Oliveira, J. Mendes-Filho, J.E. Moreira, J. Phys. C Solid State Phys. **14**, 2527 (1981)
107. A.J. Ramponi, J.C. Wright, Phys. Rev. B **31**, 3965 (1985)
108. B.S. Acharya, J. Mater. Sci. Lett. **4**, 593 (1985)
109. F.J. López, S.H. Murrieta, A.J. Hernández, O.J. Rubio, Phys. Rev. B **22**, 6428 (1980)

110. R. Pérez-Salas, T.M. Piters, R. Aceves, R. Rodríguez-Mijangos, M. Barboza-Flores, Rev. Mex. Fis. **49**, 102 (2003)
111. M.C. Marco de Lucas, F. Rodríguez, M. Moreno, Phys. Status Solidi B **172**, 719 (1992)
112. E.V. Mejía-Uriarte, R. Castañeda-Guzmán, M. Villagrán-Muniz, E. Camarillo, A.J. Hernández, S.H. Murrieta, M. Navarette, J. Phys. Condens. Matter **15**, 6889 (2003)
113. E.V. Mejía-Uriarte, E. Camarillo, A.J. Hernández, M. Navarette, M. Villagrán-Muniz, S.H. Murrieta, Opt. Mater. **27**, 1316 (2005)
114. E. Lilley, J.B. Newkirk, J. Mater. Sci. **2**, 567 (1967)
115. J.L. Gavartin, E.K. Shidlovskaya, A.L. Shluger, A.N. Varaksin, J. Phys. Condens. Matter **3**, 2237 (1991)
116. M.T. Bennebroek, A. Arnold, O.G. Poluektov, P.G. Baranov, J. Schmidt, Phys. Rev. B **54**, 11276 (1996)
117. J.S. Kasper, J.S. Prenner, Acta Crystallogr. **7**, 246 (1953)
118. P. Porta, M. Valigi, J. Solid State Chem. **6**, 344 (1973)
119. N. Valverde-Diez, D. Grande-Fernández, Solid State Ionics **28–30**, 1697 (1988)
120. P. Porta, G. Minelli, I.L. Botto, E.J. Baran, J. Solid State Chem. **92**, 202 (1991)
121. C.L. Christ, J.R. Clark, Am. Mineral. **40**, 907 (1955)
122. B. Winkler, M. Chall, C.J. Pickard, V. Milman, J. White, Acta Crystallogr. B **56**, 22 (2000)
123. J.E. Muñoz-Santiuste, J. García-Solé, M. Manfredi, Phys. Status Solidi B **163**, 191 (1991)
124. G.H. Verdiguel, C. Flores, F. Jaque, A.J. Hernández, S.H. Murrieta, J. Phys. Condens. Matter **6**, 5223 (1994)
125. A. Sors, E. Lilley, Phys. Status Solidi A **27**, 469 (1975)
126. C. Barth, C.R. Henry, New J. Phys. **11**, 043003 (2009)
127. J.J. Gilman, Trans. Am. Inst. Met. **209**, 1449 (1957)
128. J.L. Robins, T.N. Rhodin, R.L. Gerlach, J. Appl. Phys. **37**, 3893 (1966)
129. M.T. Sprackling (ed.), *The Plastic Deformation of Simple Ionic Crystals* (Academic Press, London, 1976)
130. H. Höche, H. Bethge, J. Cryst. Growth **42**, 110 (1977)
131. A.H. Ostadrahimi, H. Dabringhaus, K. Wandelt, Surf. Sci. **521**, 139 (2002)
132. J.E. Lester, G.A. Somorjai, J. Chem. Phys. **49**, 2940 (1968)
133. M.J. Yacamán, Phys. Status Solidi B **56**, 429 (1973)
134. W.A. Hofer, A.S. Foster, A.L. Shluger, Rev. Mod. Phys. **75**, 1287 (2003)
135. U. Kaiser, A. Schwarz, R. Wiesendanger, Nature **446**, 522 (2007)
136. A. Trovarelli (ed.), *Catalysis by Ceria and Related Materials*, vol. 2 (Imperial College Press, London, 2006)
137. J.V. Lauritsen, M. Reichling, J. Phys. Condens. Matter **22**, 263001 (2010)
138. C.R. Henry, Surf. Sci. Rep. **31**, 231 (1998)
139. C.R. Henry, in *The Chemical Physics of Solid Surfaces*, ed. by D.P. Woodruff, B. Elsevier, V. Warwick (UK, 2003)
140. G. Sitja, S. Le Moal, M. Marsault, G. Hamm, F. Leroy, C.R. Henry, Nano Lett. **13**, 1977 (2013)
141. M. Marsault, G. Hamm, A. Worz, G. Sitja, C. Barth, C.R. Henry, Faraday Discuss. **138**, 407 (2008)
142. Z. Gai, J.Y. Howe, J. Guo, D.A. Blom, E.W. Plummer, J. Shen, Appl. Phys. Lett. **86**, 023107 (2005)
143. M. Goryl, F. Buatier de Mongeot, F. Krok, A. Vevecka-Priftaj, M. Szymonski, Phys. Rev. B **76**, 75423 (2007)
144. M.H. Hakala, O.H. Pakarinen, A.S. Foster, Phys. Rev. B **78**, 045418 (2008)
145. J.C. Zanghi, J.J. Métois, R. Kern, Surf. Sci. **52**, 556 (1975)
146. R.B. Marcus, W.B. Joyce, Thin Solid Films **7**, R3 (1971)
147. E. Palacios-Lidon, C.R. Henry, C. Barth, ACS Catal. **4**, 1838 (2014)
148. M. Watkins, T. Trevethan, M.L. Sushko, A.L. Shluger, J. Phys. Chem. C **112**, 4226 (2008)
149. T. Trevethan, A.L. Shluger, J. Phys. Chem. C **112**, 19577 (2008)
150. Ph. Rahe, M. Kittelmann, J.L. Neff, M. Nimmrich, M. Reichling, Ph. Maass, A. Kühnle, Adv. Mater. **25**, 3948 (2013)